Ca^{2+} Binding and Conformational Changes in a Calmodulin Domain†

Johan Evenäs,* Anders Malmendal, Eva Thulin, Göran Carlström, and Sture Forsén

Physical Chemistry 2, Lund University, P.O. Box 124, S-221 00 Lund, Sweden

Received March 19, 1998; Revised Manuscript Received July 23, 1998

ABSTRACT: Calcium activation of the C-terminal domain of calmodulin was studied using ^1H and ^{15}N NMR spectroscopy. The important role played by the conserved bidentate glutamate Ca^{2+} ligand in the binding loops is emphasized by the striking effects resulting from a mutation of this glutamic acid to a glutamine, i.e. E104Q in loop III and E140Q in loop IV. The study involves determination of Ca^{2+} binding constants, assignments, and structural characterizations of the apo, $(Ca^{2+})_1$, and $(Ca^{2+})_2$ states of the E104Q mutant and comparisons to the wild-type protein and the E140Q mutant [Evenäs et al. (1997) *Biochemistry 36*, 3448−3457]. NMR titration data show sequential Ca^{2+} binding in the E104Q mutant. The first Ca^{2+} binds to loop IV and the second to loop III, which is the order reverse to that observed for the E140Q mutant. In both mutants, the major structural changes occur upon Ca^{2+} binding to loop IV, which implies a different response to Ca^{2+} binding in the N- and C-terminal EF-hands. Spectral characteristics show that the $(Ca^{2+})_1$ and $(Ca^{2+})_2$ states of the E104Q mutant undergo global exchange on a 10−100 μs time scale between conformations seemingly similar to the closed and open structures of this domain in wild-type calmodulin, paralleling earlier observations for the $(Ca^{2+})_2$ state of the E140Q mutant, indicating that both glutamic acid residues, E104 and E140, are required for stabilization of the open conformation in the $(Ca^{2+})_2$ state. To verify that the NOE constraints cannot be fulfilled in a single structure, solution structures of the $(Ca^{2+})_2$ state of the E104Q mutant are calculated. Within the ensemble of structures the precision is good. However, the clearly dynamic nature of the state, a large number of violated distance restraints, ill-defined secondary structural elements, and comparisons to the structures of calmodulin indicate that the ensemble does not provide a good picture of the $(Ca^{2+})_2$ state of the E104Q mutant but rather represents the distance-averaged structure of at least two distinct different conformations.

Calcium ions are key factors in an intracellular signaling system that translates extracellular stimuli into the regulation of a number of phenomena such as muscle contraction, cell proliferation, gene expression, and secretion processes (*1*). To accomplish such varying feats, Ca^{2+} concentration transients must be well defined in both time and space (*2*). In addition, the Ca^{2+} target proteins must be finely tuned. The most common intracellular Ca^{2+}-binding motif in proteins is the EF-hand (helix−loop−helix motif) (*3*), which normally is paired and packed against another EF-hand in a parallel fashion. Genome sequencing data have shown the EF-hand to be among the five most common protein motifs in animal cells (*4*). The 12 residue long Ca^{2+}-binding loop in a canonical EF-hand begins near the C-terminus of the incoming helix, has a conserved glycine in position 6, and forms an antiparallel β-sheet from residues in position 7−9 with the corresponding residues of the neighboring Ca^{2+}-binding loop. The last three residues in the loop start the trailing helix. The first half of the loop is essentially solvent-exposed while the second half is more buried in the protein. The 12th and last residue in the loop is a conserved glutamate residue that provides two Ca^{2+} ligands by using both carboxylate oxygens. In total there are seven Ca^{2+} ligands, with the remaining provided by the backbone carbonyl oxygen of residue 7, a water molecule, and three side-chain oxygens from residues 1, 3, and 5. The coordination geometry is usually described as a pentagonal bipyramid.

Ca^{2+}-activated calmodulin (CaM)[1] binds and regulates more than 100 different target proteins involved in a variety of cell functions (*5*−*8*). The 148 residue protein contains four EF-hands with Ca^{2+}-binding loops denoted I−IV and helices A−H. Each EF-hand pair in CaM forms a globular domain, in which the two EF-hands are connected by a linker region. The domains are linked by a flexible helical tether (*9*). Each domain binds two Ca^{2+} with positive cooperativity ($K_D \sim 10^{-6}$ M). Upon Ca^{2+} binding, the secondary structure of each domain is basically unchanged but the helices undergo a large scale reorientation, as shown by the three-dimensional structures of CaM (*10*−*14*). In the apo state the two helices in each EF-hand are roughly antiparallel yielding a closed conformation, whereas in the Ca^{2+}-loaded state the helices are more perpendicular yielding an open conformation. The rearrangements are associated with the reorganization of many side-chains and cause the exposure

† This research was supported by grants from the Swedish Natural Science Research Council. The 600 MHz NMR spectrometer was purchased by a grant from the Knut and Alice Wallenberg Foundation.

* Corresponding author. Fax: +46-46-2224543. E-mail: johan.evenas@fkem2.lth.se.

[1] Abbreviations: COSY, correlation spectroscopy; CaM, calmodulin; DQ, double quantum spectroscopy; E104Q, TR_2C with Glu 104 mutated to Gln; E140Q, TR_2C with Glu 140 mutated to Gln; HSQC, heteronuclear single-quantum coherence spectroscopy; NMR, nuclear magnetic resonance; NOE, nuclear Overhauser effect; NOESY, nuclear Overhauser effect spectroscopy; TnC, troponin C; TOCSY, total correlation spectroscopy; TR_2C, the recombinant carboxy-terminal domain of calmodulin (M76-K148); wt-TR_2C, wild-type TR_2C.

S0006-2960(98)00644-8 CCC: $15.00
Published on Web 09/05/1998

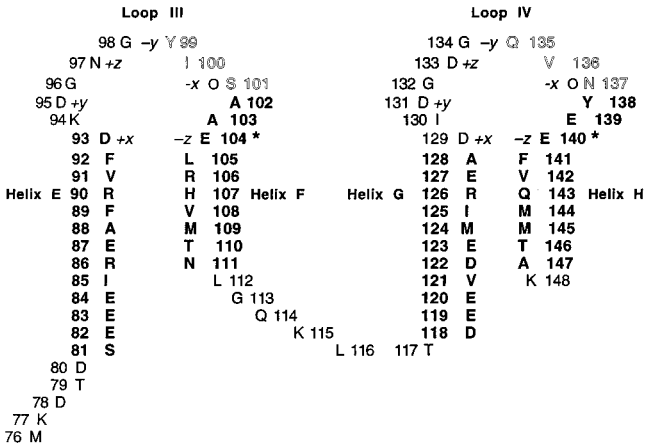

FIGURE 1: Amino acid sequence of recombinant TR_2C, the carboxy-terminal tryptic fragment of vertebrate calmodulin. Helical residues are denoted in **bold**, and residues in the β-strands are outlined. Mutation sites are indicated with an asterisk.

in each domain of hydrophobic patches that are involved in target binding. Similar structural changes are observed for homologous regulatory EF-hand proteins, e.g. skeletal muscle troponin C (TnC) (*15*−*17*). The tryptic fragments of CaM (*18*, *19*), TR_1C (A1-K77) and TR_2C (D78-K148), have been shown to be very similar to the corresponding domains of intact CaM in terms of 3D structures (*20*) as well as Ca^{2+}-binding characteristics (*21*). To reduce the complexity of the system studied, we use TR_2C for detailed investigations of Ca^{2+}-induced effects on CaM. The amino acid sequence, secondary structure, and Ca^{2+}-coordinating residues of vertebrate TR_2C are shown in Figure 1.

The structures of the apo and Ca^{2+}-saturated states of CaM and TnC (*10*−*16*) have greatly contributed to our understanding of the conformational switch in regulatory EF-hand proteins. However, many questions remain concerning the molecular mechanism behind the observed binding cooperativity and Ca^{2+}-induced structural changes. To be able to answer these questions it would be of considerable value to characterize the $(Ca^{2+})_1$ states of CaM domains. Due to the strong cooperativity of the two Ca^{2+}-binding sites in each EF-hand pair, such studies are prevented for the intact CaM as well as the individual domains, TR_1C and TR_2C. Our approach to solve the problem is to obtain sequential binding by making mutants of TR_2C where the Ca^{2+} affinity of one or the other site is decreased. The Ca^{2+}-ligating glutamic acid in the 12th position of each binding loop is replaced by a glutamine. The two resulting mutants are referred to as E104Q and E140Q. Earlier studies of such mutations of CaM and other EF-hand proteins have shown large effects on protein properties (*22*−*26*), e.g. altered Ca^{2+} affinities and ability of activating target proteins. The observed reduction in Ca^{2+} affinity is attributed mainly to an increased off-rate (*27*), which causes the C-terminal domain mutants to exhibit fast Ca^{2+} exchange on the ^1H NMR chemical shift time scale instead of the slow-exchange behavior observed for wild-type TR_2C (wt-TR_2C).

Recently, we reported structural and Ca^{2+} binding characteristics of E140Q using ^1H and ^{15}N NMR spectroscopy (*28*). To briefly summarize those findings, the apo states of wt-TR_2C and E140Q seem very similar. However, the Ca^{2+} affinities of loop III and IV in E140Q are reduced by approximately 2 and 4 orders of magnitude, respectively, and the Ca^{2+} binding is essentially sequential. The binding of the first Ca^{2+} to loop III does not seem to induce any major structural changes while binding of the second Ca^{2+} gives rise to large global structural changes. $(Ca^{2+})_2$ E140Q seems to experience conformational exchange on a 10−100 μs time scale between at least two states, corresponding to a closed and an open conformation structurally similar to apo and $(Ca^{2+})_2$ wt-TR_2C, respectively. This conclusion is based on observations of two sets of mutually exclusive NOEs that conform with the apo and $(Ca^{2+})_2$ wt-TR_2C structures. In addition, a large number of resonance lines are broadened by exchange processes other than Ca^{2+} exchange, and the majority of the chemical shifts appear at values between those of apo and $(Ca^{2+})_2$ wt-TR_2C. ^{15}N spin relaxation studies of $(Ca^{2+})_2$ E140Q confirm the existence of global exchange processes (Evenäs, Forsén, and Akke, unpublished results).

The present study describes the Ca^{2+}-binding properties and structural features of E104Q in the different states using ^1H and ^{15}N NMR spectroscopy. The results are compared with those for wt-TR_2C and E140Q. Since the mutations are performed at equivalent positions in each EF-hand, differences observed for the mutants can be attributed to different properties of the two EF-hands. Observed properties common to both mutants, but not to wt-TR_2C, give mutation-specific information and shed light on the role of the bidentate Ca^{2+}-ligating glutamic acids.

EXPERIMENTAL PROCEDURES

Synthesis of Mutant, and Protein Production. A synthetic gene of the C-terminal domain of vertebrate CaM (M76-K148), TR_2C, was constructed from overlapping oligonucleotides (Brodin, unpublished) essentially as described for bovine calbindin D_{9k} (*29*). The mutation was made with the mismatch method using the kit MUTA-GENE M13 In Vitro Mutagenesis from BIORAD. The glutamic acid in position 104 was replaced by a glutamine by changing the codon from GAA to CAA using an oligonucleotide with a length of 21 bases. The E104Q gene was cloned into the runaway plasmid pRCB1. Expression and purification of unlabeled and ^{15}N-labeled E104Q was carried out as previously described for wt-TR_2C (*20*).

NMR Sample Preparation. For all NMR samples, apo E104Q was dissolved to concentrations of 1−4 mM in H_2O (10% D_2O) and 0.1 mM NaN_3. The first sample in the titration series had a protein concentration of 1.16 mM. Desired amounts of Ca^{2+} were added to the samples as aqueous solutions of $CaCl_2 \cdot 2\ H_2O$. In all samples, pH was adjusted to 6.00 ± 0.05 with 0.1 M KOH and HCl.

NMR Spectroscopy, Data Processing and Analysis. All NMR experiments were performed at 28 °C. Water suppression was obtained by weak presaturation for 1.3 s in ^1H NMR experiments. COSY (*30*) and NOESY (*31*, *32*) spectra of apo E104Q were acquired using a GE Omega 500 spectrometer operating at 500.13 MHz. The NOE mixing time was 200 ms. All other experiments were run on a 600 MHz Varian UNITY PLUS spectrometer. The following ^1H NMR spectra of the $(Ca^{2+})_1$ state of E104Q were recorded: COSY, DQ (30 ms) (*33*), TOCSY (75 ms) (*34*) using the DIPSI-2 isotropic mixing sequence (*35*), and NOESY (150 ms). Recorded spectra of $(Ca^{2+})_2$ state were

COSY, NOESY (150 ms), and a 2D ^{15}N HSQC-TOCSY (90 ms) using the DIPSI-2rc isotropic mixing sequence (*36*).

Sensitivity-enhanced ^{1}H−^{15}N HSQC spectra of E104Q, at various Ca^{2+} levels, were recorded using a pulse sequence with gradient selection and a water-flip-back pulse (*37*). The spectra were recorded with 64 and 2048 complex data points in t_1 and t_2, respectively, and a relaxation delay of 1.3 s. The ^{15}N nuclei were decoupled during acquisition using the WALTZ-16 sequence (*38*). The spectral widths were 1600 and 8000 Hz in the ^{15}N dimension and ^{1}H dimension, respectively, with 16 scans per t_1 increment. All spectra were processed using Felix95 (MSI Inc.).

Ca^{2+} Titration, and Binding Constants of E104Q. A series of ^{1}H−^{15}N HSQC spectra was acquired to monitor Ca^{2+} titration of E104Q at 15 different Ca^{2+} concentrations ranging from 0 to 28 equiv of Ca^{2+} relative to the protein. The Ca^{2+} and protein concentrations at the final titration point were determined by atomic absorption spectrophotometry and amino acid hydrolysis, respectively.

The macroscopic binding constants were calculated using a simulated annealing protocol, described earlier (*28*). Briefly, the binding constants, K_1 and K_2, and the chemical shifts of the $(Ca^{2+})_1$ and $(Ca^{2+})_2$ states for each amide nucleus j, $\delta_{Ca1}(j)$ and $\delta_{Ca2}(j)$, were determined by simultaneous fitting to the observed chemical shifts of 25 arbitrarily chosen nuclei exhibiting fast exchange at the different Ca^{2+} concentrations, i. In all 52 variables were determined by minimizing the function

$$\sum_{i}^{15}\sum_{j}^{25}\{[I - p_{Cal}(i) - p_{Ca2}(i)]\delta_{apo}(j) + p_{Ca1}(i)\delta_{Ca1}(j) + p_{Ca2}(i)\delta_{Ca2}(j) - \delta_{obs}(i,j)\}^2 \quad (1)$$

where $p_{Ca1}(i)$ and $p_{Ca2}(i)$ are the relative populations of the $(Ca^{2+})_1$ and the $(Ca^{2+})_2$ states, calculated via K_1, K_2, and the protein and Ca^{2+} concentrations, and $\delta_{obs}(i,j)$ is the observed chemical shift for nucleus j at Ca^{2+}-concentration i. The chemical shifts of the apo state, δ_{apo}, were obtained directly from the HSQC spectrum recorded prior to adding Ca^{2+}.

NMR Assignment. ^{1}H chemical shifts were referenced to the $^{1}H_2O$ signal at 4.725 ppm at 301 K (*39, 40*). ^{15}N chemical shifts were referenced using the frequency ratio (^{15}N/^{1}H) of 0.101 329 118 where the ^{1}H frequency is that of DSS (0 ppm) in H_2O (*41*). The assignments were performed using GENXPK (*42*), which allowed prediction and monitoring of cross-peak locations, in conjunction with Felix95. Complete backbone and side-chain ^{1}H and ^{15}N assignments of apo, $(Ca^{2+})_1$, and $(Ca^{2+})_2$ E104Q were obtained using the NMR spectra of each state. The apo assignment was facilitated by the close resemblance to the assignments of wt-TR_2C and E140Q (*28, 43*), and by following the cross-peaks in HSQC spectra of the Ca^{2+} titration, the amide nuclei of $(Ca^{2+})_2$ E104Q were readily assigned. Using the amide-proton-based strategy (*44*), $(Ca^{2+})_1$ E104Q was assigned at a Ca^{2+} level such that the $(Ca^{2+})_1$ state was populated to 88%. The NOE assignments were straightforward using GENXPK and the in-house ASSar program.

The amide chemical shifts of the pure $(Ca^{2+})_1$ state were also calculated using the Ca^{2+} titration data. If one neglects effects from increased ionic strength and additional non-specific Ca^{2+} binding, the observed chemical shift, δ_{obs}, at a certain Ca^{2+} concentration for a nucleus exhibiting fast exchange is given by

$$\delta_{obs} = (1 - p_{Ca1} - p_{Ca2})\delta_{apo} + p_{Ca1}\delta_{Ca1} + p_{Ca2}\delta_{Ca2} \quad (2)$$

where p_{Ca1} and p_{Ca2} are the relative populations of the $(Ca^{2+})_1$ and $(Ca^{2+})_2$ states, calculated at each titration point from the fitted values of the binding constants and the known protein and Ca^{2+} concentrations. Using eq 2 we obtained values of the chemical shifts of the $(Ca^{2+})_1$ and $(Ca^{2+})_2$ states, δ_{Ca1} and δ_{Ca2}, from each individual binding curve. The approach must be considered as an approximation for nuclei having broadened resonance lines, since the chemical shift of a nucleus in intermediate exchange between unequally populated states depends on the exchange rates (*45*). Furthermore, any conformational exchange behavior of the different states of E104Q is assumed to be independent of the Ca^{2+} concentration; i.e. the chemical shift of each state does not vary with the Ca^{2+} concentration.

Structure Calculations. Structure calculations of $(Ca^{2+})_2$ E104Q were carried out using X-PLOR 3.1 (*46*). Initial structures were obtained using distance geometry (DG) embedding without metrization. Restrained simulated annealing and refinement were subsequently performed using the standard protocols (*46, 47*). For equivalent and non-stereospecifically assigned atoms, distance restraints were input as $(\Sigma r^{-6})^{-1/6}$ (*48*). No hydrogen bond constraints were used during the structure calculations.

Distance restraints were derived from the cross-peak intensities obtained from the NOESY spectrum with a mixing time of 150 ms, possibly suffering from spin diffusion, and grouped into four conservatively chosen classes: 1.8−3.0 Å (strong), 1.8−3.7 Å (medium), 1.8−4.4 Å (weak), and 1.8−5.5 Å (very weak). To correct for internal motions of methyl protons, 0.3 Å was added to the upper bound of these restraints (*49, 50*). Overlapped NOE cross-peaks were treated as very weak restraints. The final structures were calculated using 1104 distance restraints (368 intraresidue, 271 sequential, 233 medium range, and 232 long range) and 32 dihedral angle restraints derived from $^{3}J_{NH\alpha}$ coupling constants. For several residues, backbone dihedral angle restraints could not be derived due to broadened amide proton lines. To ensure that no structures precluded Ca^{2+} binding, 10 restraints were used between the calcium ions and their protein ligands, among those restraints to the residue in the twelfth loop position. These restraints were based on Ca^{2+} coordination in the 3D structure of $(Ca^{2+})_4$ CaM (*10*). 50 structures of $(Ca^{2+})_2$ E104Q were generated with 100% rate of convergence. All refined structures were chosen for further analysis.

RESULTS

NMR spectroscopy has been used to obtain the chemical shift assignments and to structurally characterize the apo, $(Ca^{2+})_1$, and $(Ca^{2+})_2$ states of E104Q in order to investigate the Ca^{2+}-induced activation of CaM and the importance of the conserved glutamic acid residue in the binding loop that functions as a bidentate Ca^{2+} ligand. Careful analysis of NMR titration data provides information on the effects of Ca^{2+} binding in E104Q at an atomic resolution. The ^{15}N and HN chemical shifts of the different states are supplied as Supporting Information.

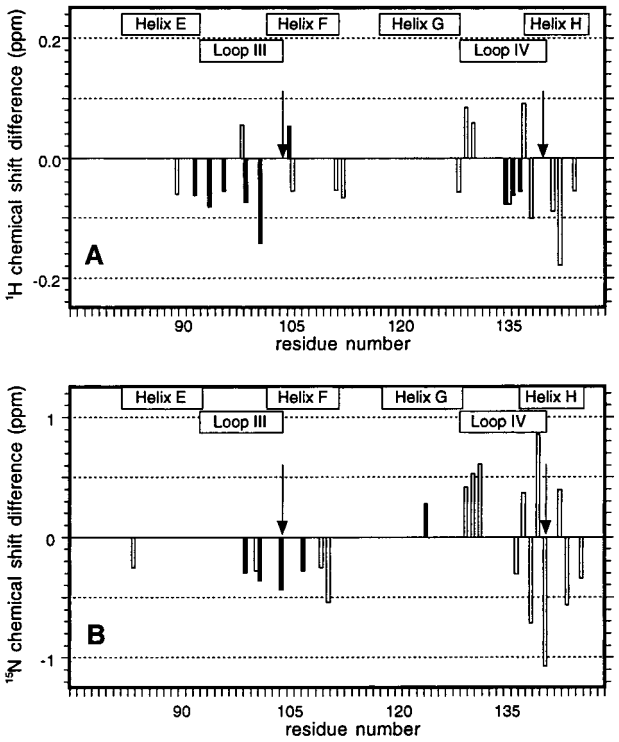

FIGURE 2: Chemical shift differences between the apo states of mutants and wt-TR_2C for backbone amide nuclei at 301 K and pH 6.0. ^{1}H chemical shift differences, >0.05 ppm, are shown in panel A, and ^{15}N chemical shift differences, >0.25 ppm, in panel B. Filled bars correspond to differences between E104Q and wt-TR_2C and open bars to differences between E140Q and wt-TR_2C. Locations of Ca^{2+}-binding loops and helices are indicated at the top, and the arrows indicate the two mutation sites.

Apo E104Q. Figure 2 displays the chemical shift differences of the backbone amide nuclei between the apo states of E104Q, E140Q, and wt-TR_2C, showing that the E104Q mutation causes only minor changes (filled bars), similar to previous results for E140Q (open bars) (*28*). Even though it is difficult to rationalize chemical shift changes in terms of changes at a level of atomic resolution, the results indicate that the mutation causes only small perturbations of structure and dynamics of the apo state.

No chemical shift of E104Q deviates from wt-TR_2C by more than 0.2 and 0.5 ppm for amide protons and nitrogens, respectively (Figure 2). The largest differences relative to wt-TR_2C are seen for residues in the β-sheet region, Y99-S101 and Q135-N137, and for a few other residues in loop III. The effects on the β-sheet region may be caused by a different hydrogen-bonding interaction between the side chain of Q104 and the amide proton of S101. The effects on the chemical shifts are generally slightly smaller and more localized than those observed for E140Q.

Ca^{2+} Binding to E104Q. The chemical shift changes of the amide nuclei of ^{15}N-labeled E104Q as a function of Ca^{2+} concentration were obtained from 15 HSQC spectra, recorded at different Ca^{2+} concentrations up to 28 equiv relative to the protein. The well-resolved spectra show that the NMR spectral changes generally occur in the fast- to intermediate-exchange regime on the ^{1}H and ^{15}N NMR chemical shift time scales, depending on the size of Ca^{2+}-induced chemical shift changes (*45*). However, intermediate- to slow-exchange behavior is observed for several cross-peaks in loop IV (G132, G134, Y138, E140, and F141) upon binding of the first Ca^{2+} to that loop. Twelve ^{15}N−HN cross-peaks are broadened beyond detection for intermediate Ca^{2+} concentrations, presumably due to Ca^{2+} exchange.

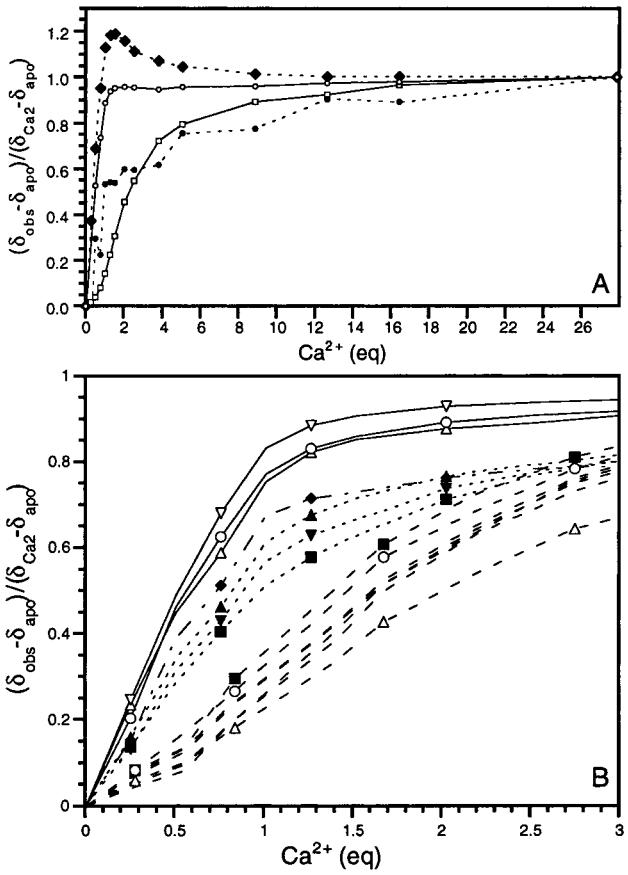

FIGURE 3: Ca^{2+}-binding curves of amide nuclei at 301 K and pH 6.0. Each curve is normalized according to $(\delta_{obs} - \delta_{initial})/(\delta_{final} - \delta_{initial})$. Panel A shows binding curves of some amide nuclei of E104Q: R90HN (◆), N97HD2 (□), N111ND (●) and I130N (○). In panel B the averages of the normalized curves for each structural element are displayed. For E140Q, the number of binding curves used for each average of E104Q is 6, 15, 11, 8, 3, 6, and 6 for helix E, loop III, helix F, linker, helix G, loop IV, and helix H, respectively. Dotted and solid lines are used for the structural elements in the N-terminal and C-terminal EF-hand in E104Q, respectively. A dashed−dotted line is used for the linker. Dashed lines are used for the curves for all structural elements of E140Q. The following symbols are used for the structural elements: helix E (▲), loop III (■), helix F (▼), linker (◆), helix G (△), loop IV (○), and helix H (▽). T-tests show that the curves of helix H and loop IV of E104Q are statistically different at a 95% confidence interval from all the curves of the N-terminal EF-hand and the linker.

The binding curves (Figure 3) exhibit biphasic profiles due to two sequential Ca^{2+}-binding events in E104Q. The binding order is shown by the larger relative chemical shift changes for nuclei in loop IV than for nuclei in loop III, generally observed upon addition of the first Ca^{2+} equivalent. The macroscopic binding constants, K_1 and K_2, are assumed to be equal to the site-specific microscopic binding constants, k_{IV} and $k_{III,IV}$, respectively (*21*), where k_{IV} is the binding constant of loop IV when loop III is empty and $k_{III,IV}$ is the binding constant of loop III when loop IV is occupied. The logarithms of the binding constants, $^{10}\log(K_1)$ and $^{10}\log(K_2)$, were determined to 5.3 ± 0.2 and 2.94 ± 0.06, respectively. Thus, the Ca^{2+} affinities of both loops are notably affected by the mutation, as was also found for E140Q (Table 1). In

Table 1: Macroscopic Ca^{2+} Binding Constants and Maximal Population of the $(Ca^{2+})_1$ States in wt-TR_2C, E104Q, and E140Q at 301 K and pH 6.0

protein	$^{10}\log(K_1/M^{-1})$	$^{10}\log(K_2/M^{-1})$	max population of the $(Ca^{2+})_1$ state[a]/%
wt-TR_2C[b]	6.9 ± 0.2	7.7 ± 0.2	0[c]
E104Q	5.3 ± 0.2	2.94 ± 0.06	88
E140Q	4.5 ± 0.2[d]	3.15 ± 0.10	70

[a] Assuming 1 mM protein, i.e. NMR conditions. [b] Data obtained at 298 K and pH 7.5 (*21*). [c] No $(Ca^{2+})_1$ state can be observed due to the strong cooperativity. [d] Previously determined to 4.9 ± 0.3 by using NMR (*28*). The more accurate value was obtained by using near-UV CD spectroscopy (data not published).

addition, K_1 was determined from a titration monitored by UV absorption spectroscopy in the presence of a competitive fluorescent Ca^{2+}-binding chelator (*51*). This method yields a value of $^{10}\log(K_1) = 5.2 \pm 0.3$, in good agreement with the one obtained from the NMR data. A maximal population of the $(Ca^{2+})_1$ state of 88% at 1.07 equiv of Ca^{2+} is implied from the binding constants under NMR conditions. The final titration point, with 28 equiv of Ca^{2+} (28 mM Ca^{2+}) corresponds to 96% $(Ca^{2+})_2$ E104Q.

Each Ca^{2+}-binding event results in chemical shift changes all over the protein. The result is a heterogeneous ensemble of binding curves where the course of each curve depends on the role and the surroundings of the individual nucleus in the different Ca^{2+} states. To facilitate a comparison, all binding curves were normalized using the initial and final chemical shift values. We examined only curves for which the absolute chemical shift difference between the apo and $(Ca^{2+})_2$ states exceeds 0.12 ppm (^{1}H) and 0.6 ppm (^{15}N) to avoid pronounced effects from increased ionic strength (up to ~30 mM $CaCl_2$) and experimental uncertainties. Ionic strength effects are particularly notable for residues in the N-terminus, the linker, and helix G. Figure 3A shows examples of normalized curves. A few nuclei experience chemical shift changes of opposite signs from the two Ca^{2+}-binding events, clearly illustrating the sequential binding, e.g. R90HN. Unexpected zigzag curves were obtained for N111ND (Figure 3A) and H107HN. The behavior can be explained by small variations in pH which changes the degree of protonation of the imidazole ring of H107. The pK_a values for the ring are reported to be 6.48 and 6.10 for apo and $(Ca^{2+})_4$ CaM, respectively (*52*).

To establish if the different structural elements (helices E−H, binding loops II−IV, and the linker region) of E104Q respond differently to the two Ca^{2+} binding events, the average curve of each structural element was calculated from the normalized binding curves. The average curves are shown in Figure 3B, compared with the corresponding curves for E140Q. Upon binding of the first Ca^{2+} to loop IV in E104Q, large shift changes are observed in all regions of the protein, indicating global structural effects. In addition, the binding order is illustrated by the two distinct categories of binding curves; i.e. the structural elements of the C-terminal EF-hand (helices G and H and loop IV) show a significantly steeper initial response than those of the N-terminal EF-hand (helices E and F and loop III) (Figure 3B). The relative order of the response of the different structural elements of the N-terminal EF-hand, helix E > helix F > loop III, seems reasonable since helix E is

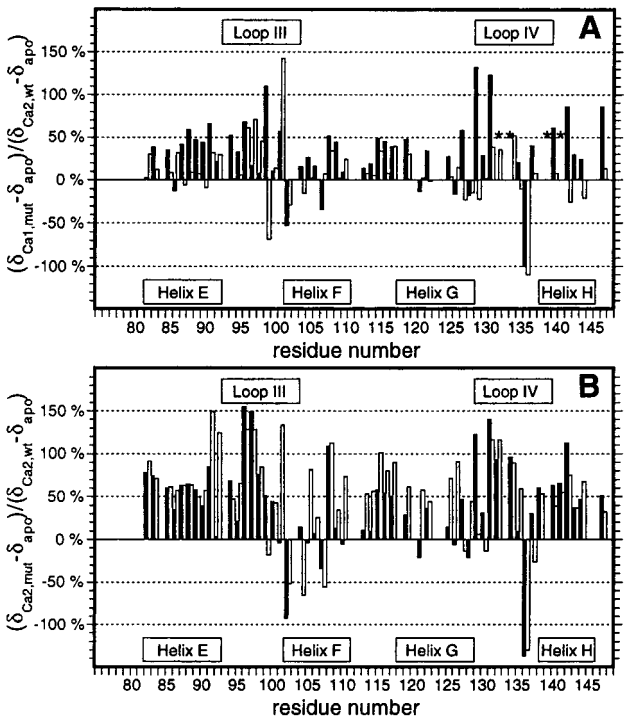

FIGURE 4: Ca^{2+}-induced chemical shift changes of the backbone amide protons of E104Q (filled bars) and E140Q (open bars) expressed in percentage of the chemical shift difference between the $(Ca^{2+})_2$ and apo state of wt-TR_2C at 301 K and pH 6.0. Wild-type ^{1}H chemical shift differences range up to ~1.7 ppm with the largest values in the binding loops. Panel A shows the relative changes upon binding of the first Ca^{2+} to E104Q and E140Q $(\delta_{Ca1,mut} - \delta_{apo,mut})/(\delta_{Ca2,wt} - \delta_{apo,wt})$, and panel B, the changes for binding of both Ca^{2+} $(\delta_{Ca2,mut} - \delta_{apo,mut})/(\delta_{Ca2,wt} - \delta_{apo,wt})$. Bars are only shown for residues for which the chemical shift change in wt-TR_2C exceeds 0.12 ppm, to avoid errors due to slightly different sample conditions. Residues exhibiting slow−intermediate exchange are omitted and indicated with asterisks. Locations of helices and Ca^{2+}-binding loops are indicated at the bottom and the top.

intimately connected to helix H in the C-terminal EF-hand via hydrophobic residues. The binding curve of the linker is found between those of the EF-hands.

The results indicate substantial differences between Ca^{2+} activation of E104Q and E140Q (Figure 3B). In E140Q, only minor changes occur upon binding of the first Ca^{2+} to loop III (*28*). Two categories of binding curves for the two EF-hands are not observed for E140Q where the first Ca^{2+} binding to loop III causes almost equal shift changes in both binding loops, while the helices and linker respond less strongly.

$(Ca^{2+})_1$ E104Q. The amide chemical shifts of the $(Ca^{2+})_1$ state were calculated from a fit of the binding curves to eq 2. Theoretical binding curves calculated from these chemical shifts show in general excellent agreement with the experimental curves. Due to kinetic effects on the chemical shift, deviations for nuclei exhibiting intermediate exchange are notable, particularly for G132 and G134. $(Ca^{2+})_1$ chemical shifts for nuclei exhibiting slow to intermediate exchange are not included in Figure 4A or the Supporting Information. Less good fits were also found for some nuclei in the N-terminus and the start of helix G. A possible explanation may be that these residues experience chemical shift effects from the increased ionic strength that are significant compared to the Ca^{2+}-induced shift changes.

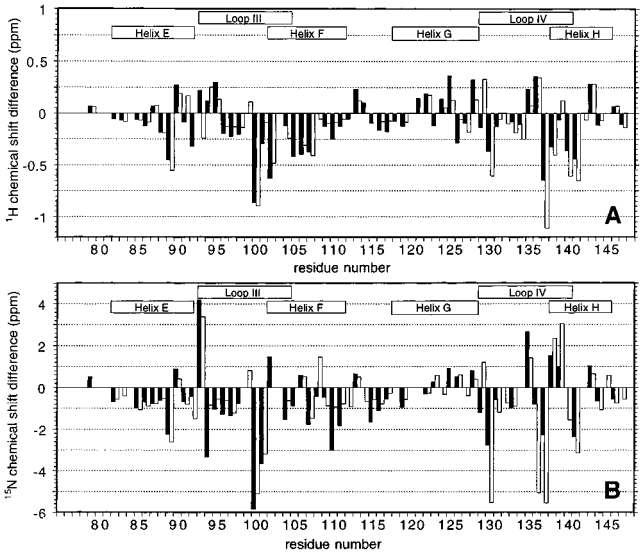

FIGURE 5: Chemical shift differences between the $(Ca^{2+})_2$ states of mutants and wt-TR_2C for amide nuclei at 301 K and pH 6.0. Filled bars correspond to differences between E104Q and wt-TR_2C, and open bars, to differences between E140Q and wt-TR_2C. Panels A and B show differences between backbone amide protons and nitrogens, respectively. Locations of the helices and Ca^{2+}-binding loops are indicated at the top.

In Figure 4A we show the ratio of the backbone amide chemical shift changes caused by the first Ca^{2+} binding event in E104Q (filled bars) and E140Q (open bars) to the total chemical shift change from the apo state to the $(Ca^{2+})_2$ state in wt-TR_2C. Figure 4A clearly shows the large chemical shift response to binding of the first Ca^{2+} to E104Q, as compared to E140Q. In the C-terminal EF-hand of E104Q, which binds the first ion, many nuclei display a pronounced chemical shift change toward the values of the $(Ca^{2+})_2$ state of wt-TR_2C. Similar, but smaller, changes are also observed for protons in the region comprising helix E and the first part of empty loop III (D93-G98) and in the linker. No clear trends are, however, identified for the β-sheet and helices F and G where protons in general exhibit smaller, in some cases, opposite chemical shift changes compared to wt-TR_2C.

NMR spectra were recorded at conditions such that the $(Ca^{2+})_1$ state was populated to 88%, and the remaining 12% were equally distributed between the apo and $(Ca^{2+})_2$ state. The aim was to characterize the Ca^{2+}-induced structural changes in $(Ca^{2+})_1$ E104Q by careful investigations of the NOESY spectrum. Close to complete ^{1}H and ^{15}N assignment was obtained despite broadening of several amide resonances. The amide proton of N97 was broadened beyond detection. In general, the assignment shows good agreement with the chemical shifts of the pure $(Ca^{2+})_1$ state calculated from the fit of the binding curves (cf. above). The NOEs indicate, however, that the $(Ca^{2+})_1$ state experiences conformational exchange. For convenience, these results are discussed below in conjunction with the presentation of the similar results obtained for $(Ca^{2+})_2$ E104Q.

$(Ca^{2+})_2$ E104Q. Backbone amide chemical shift differences between the mutants and wt-TR_2C are shown in Figure 5—note the large shift scale used compared to Figure 2. In contrast to the apo state, many chemical shifts of $(Ca^{2+})_2$ E104Q differ significantly from wt-TR_2C, particularly in the loops, helix F, and the aromatic regions (F89-D93 and Y138-V142). The $(Ca^{2+})_2$ states of the E104Q and E140Q show surprisingly similar shift deviations (Figures 4B and 5). Although the two mutations are performed at equivalent positions in the two loops, their distant locations nevertheless makes the observed similarity intriguing.

In $(Ca^{2+})_2$ wt-TR_2C, stabilizing hydrogen bonds are formed from the backbone amide protons of residues 2 and 7 in the binding loop to the side-chain oxygens of residue 12, i.e. from K94, S101, to E104 in loop III and from I130, N137, to E140 in loop IV. Perturbations of these hydrogen bonds due to the mutations seem to cause site-specific chemical shift differences between the mutants. The amide nitrogen of K94 is greatly shifted upfield in E104Q as is the nitrogen of I130 in E140Q. Less pronounced upfield shifts are also observed for the amide proton of the same residues. An upfield shift of an amide proton is typical for a weakened or absent hydrogen bond of that proton. The interpretation of a decrease in hydrogen bond strengths in the mutated loop is further supported by the more upfield shifts of S101HN and N137HN in E104Q and E140Q, respectively.

Structural Characterization of $(Ca^{2+})_1$ and $(Ca^{2+})_2$ E104Q. Identification of a large number of sequential and medium-range NOE cross-peaks in the 2D ^{1}H NOESY spectra showed that the secondary structure of wt-TR_2C is preserved in the $(Ca^{2+})_1$ and $(Ca^{2+})_2$ states. In the case of the long-range NOEs, a different pattern, however, became apparent. For both states, the unambiguously assigned long-range NOEs can be divided into three sets. One set involves NOEs between protons that are spatially close (<5 Å) in both the closed apo and the open $(Ca^{2+})_2$ structures of wt-TR_2C. The other two sets consist of mutually exclusive NOEs that are typical of only one or the other of the two structures. Each of these latter two sets consists of at least 45 NOEs between protons at various locations in the protein. The NOE intensities for a certain distance value are of the similar magnitudes in the two sets. This implies that the two sets in the NOESY spectrum of $(Ca^{2+})_2$ E104Q cannot represent the $(Ca^{2+})_1$ and the $(Ca^{2+})_2$ state, respectively, since the $(Ca^{2+})_1$ state is populated to only 4%. Likewise, for $(Ca^{2+})_1$ E104Q, the $(Ca^{2+})_1$ state must cause these two sets of NOEs, since the apo and $(Ca^{2+})_2$ state each is populated to only 6%. In addition, 8 and 6 long-range NOEs of low intensity, expected in neither the closed or open state of wt-TR_2C, were found for $(Ca^{2+})_1$ and $(Ca^{2+})_2$ E104Q, respectively.

For both $(Ca^{2+})_1$ E104Q and $(Ca^{2+})_2$ E140Q, many NOEs in the two sets involve well-resolved resonances from the aromatic side-chains in the hydrophobic core, i.e. F89 and F92 in the C-terminus of helix E and Y138 and F141 in the N-terminus of helix H. Upon Ca^{2+} binding, these side-chains rearrange and form an aromatic cluster in wt-TR_2C, and two distinct patterns of NOEs are expected for the closed and open structures. Cross-peaks typical of the two states are also found between nuclei of other nonaromatic residues. Interestingly, in $(Ca^{2+})_1$ E104Q NOEs characteristic of the open conformation are primarily found in the C-terminal EF-hand, where the Ca^{2+} is bound, or between the EF-hands, while few are found in the mutated N-terminal EF-hand. A similar, but less evident, NOE pattern is also established for the $(Ca^{2+})_2$ state. These findings may partially be explained by the fact that NOEs characteristic of an open conformation are scarce within the N-terminal EF-hand—these observations were made during structure calculations of $(Ca^{2+})_2$ wt-TR_2C (*20*). As in the case of $(Ca^{2+})_2$ E140Q, the $(Ca^{2+})_1$ and

$(Ca^{2+})_2$ states of E104Q seem to experience exchange between a closed and an open conformation (*28*). In addition to the similarities in chemical shifts of the $(Ca^{2+})_2$ states of E104Q and E140Q, the broadening patterns of the resonance lines are also similar. As in the case of E140Q (*28*), the line broadening cannot be caused by Ca^{2+} exchange but must be due to other exchange processes at a 10−100 μs time scale. The broadened resonances are most evident for nuclei in the β-sheet and for hydrophobic residues. When Ca^{2+} binds to CaM, the C-terminus of helix E exhibits a switch from a 3_{10}- to a α-helical conformation (*13, 14, 20*). Amide proton resonance lines corresponding to this region are broadened in the NMR spectra of $(Ca^{2+})_2$ E104Q, possibly indicating an exchange between these helical conformations. A conformational exchange implies that the observed chemical shifts are population-weighted averages of the shifts in different populated conformations. Such a dynamic structural switch offers an explanation for the large shift deviations between the $(Ca^{2+})_2$ states of the mutants and wt-TR_2C.

To estimate the populations of the closed and open states, a semiquantitative analysis of the NOE intensities is performed. We assume a two-state model of the exchange and the same relaxation rates in both states. If one neglects spin diffusion effects, local variations of the internal dynamics in the two states, and minor populations of states with other levels of Ca^{2+} saturation, the intensity of a particular NOE can be approximated by

$$I_{NOE} = C\left(\frac{p_c}{r_c^6} + \frac{p_o}{r_o^6}\right) \quad (3)$$

where r_c and r_o is the effective NOE distance between the protons of interest in the closed and open states, respectively, and p_c and p_o are the corresponding populations. Using eq 3 we may estimate p_c and p_o using distances derived from the 3D structures of apo CaM (*13*) and $(Ca^{2+})_4$ CaM (*10*). An important source of error is that the distances in our closed and open states are not likely to correspond precisely to those of the wild-type states; e.g. a 10% longer distance would cause a 44% decrease in the intensity. Populations of 65% and 75% were calculated for the open conformation for $(Ca^{2+})_1$ and $(Ca^{2+})_2$ E104Q, respectively. A similar estimate based on the observed chemical shifts of the $(Ca^{2+})_1$ and $(Ca^{2+})_2$ forms of E104Q is uncertain, since even if the closed conformation is similar to the apo structure of wt-TR_2C, the chemical shifts are likely to be different due to the presence of bound Ca^{2+}—in particular for nuclei in or close to the binding loops. Assuming that amide chemical shifts for residues far from the Ca^{2+}-binding loops can be represented by population-weighted averages of the chemical shifts of apo and $(Ca^{2+})_2$ wt-TR_2C, values of 33% and 42% of the open conformation were calculated for $(Ca^{2+})_1$ and $(Ca^{2+})_2$ E104Q, respectively. Evidently, large errors are associated with both approaches, but the results still indicate that the populations of the closed and open state are roughly equal in both $(Ca^{2+})_1$ E104Q and $(Ca^{2+})_2$ E104Q. The different population estimates translate into a modest difference in K_{eq} and, therefore, in ΔG between the open and closed states.

Structure Calculation of $(Ca^{2+})_2$ *E104Q.* Since we observe two sets of NOEs, characteristic of either a closed or an open conformation, as well as line broadening of many resonances—seemingly caused by exchange between the closed and open states—distinct different conformations of $(Ca^{2+})_2$ E104Q are very likely to exist. Intuitively, this is expected to lead to a large number of violations in structure calculations. However, to exclude the possibilities of another unique conformation fulfilling all of the restraints simultaneously, structure calculations were undertaken, ignoring all evidence for the conformational exchange in $(Ca^{2+})_2$ E104Q. The final ensemble of 50 refined structures exhibits fairly good precision, with an rms deviation of 1.17 Å for the backbone atoms of the well-folded part (E82-M145). For 0, 17 and 25 out of the 50 structures, the maximal violation of all restraints are <0.4, <0.5, and <1 Å, respectively. A total of 46 restraints are violated > 0.2 Å in more than 10 structures. Most of the violated restraints belong to either of the two sets of "mutually exclusive" NOEs. To assess the quality of the 50 structures we used Procheck (*53*). Analysis of pairs of ϕ and ψ angles shows that 68%, 92%, 96%, and 4% of the residues fall into the most favored, allowed, generously allowed, and disallowed regions of the Ramanchandran diagram which indicates an acceptable, but not good, quality in this respect. Furthermore, the β-strands as well as helix G are extremely ill-defined in the large majority of calculated structures according to the Procheck criteria. It is, however, likely that these elements are present in $(Ca^{2+})_2$ E104Q.

The fold of the calculated structure is essentially closed but there are evident differences to the apo structure of wild-type calmodulin (*13, 14, 20*); e.g., helix F is slightly bent and differently oriented. Comparisons to the structures of the C-terminal domain of apo and $(Ca^{2+})_4$ wild-type CaM show that the mutated N-terminal EF-hand seems more apo-like while the region around helix G and loop IV looks more similar to the open state of $(Ca^{2+})_2$ wt-TR_2C. It should be noted that since few interhelical NOEs occur within an open EF-hand, a bias toward a closed conformation is expected. Many hydrophobic side-chains in the core of the protein are observed to be oriented between the orientations observed in the closed and open conformations of wt-TR_2C, respectively. These orientations seem caused by the obligations to satisfy the distance restraints characteristic for either the closed or open conformation. Well-defined side-chains are not unexpected in structure calculations of a protein when the NOE cross-peaks reflect two or more conformations simultaneously (*54*−*56*). This might lead into situations where side-chains are pinned in unrealistic conformations when all restraints have to be fulfilled at the same time. The many violations of distance restraints, the distorted β-strands and helix G, the bent helix F, and the apparently over-constrained structures indicate strongly that the ensemble is not sufficiently relevant for $(Ca^{2+})_2$ E104Q as discussed below.

DISCUSSION

In studies of cation-induced effects on mutated cation binding proteins at intermediate saturation levels, it is important to distinguish between effects of cation binding and mutational artifacts. The two are often intimately coupled and hard to separate. One important prerequisite is that the mutation does not significantly affect the protein structure in the cation-free state. The small chemical shift

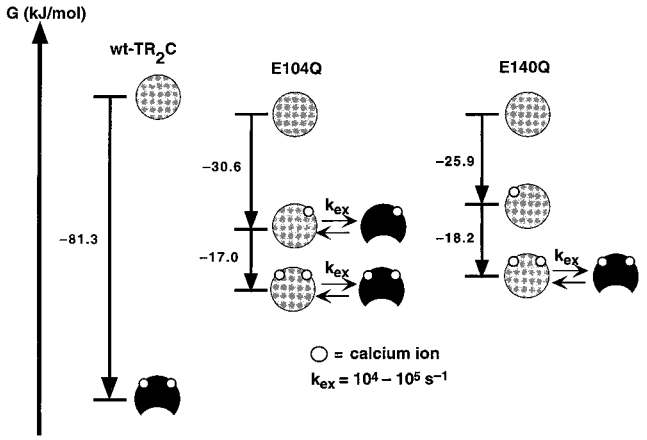

FIGURE 6: A schematic view of the conformations and relative free energies of the different apo and Ca^{2+}-bound states of wt-TR_2C and the two mutants, E104Q and E140Q. The free energy changes are calculated using $\Delta G = -RT \ln K$, where K is the binding constant of each Ca^{2+}-binding event and $T = 301$ K.

changes for E104Q as well as E140Q relative to wt-TR_2C indicate that this is fulfilled (Figure 2).

Ca^{2+} Binding to E104Q, E140Q and wt-TR_2C. As will be further discussed below, our NMR data indicate that the $(Ca^{2+})_2$ forms of E104Q and E140Q experience exchange between closed and open conformations. Keeping in mind the dynamic nature of the end states, we interpret the NMR Ca^{2+} titration data in structural and thermodynamical terms. In Figure 6 we summarize the conformations of each state of wt-TR_2C and the mutants in a free energy diagram. The relative energies of the apo states may seem arbitrary. Preliminary calorimetric measurements indicate, however, that the apo states of the mutants are more stable than apo wt-TR_2C (Peter Sellers, personal communication). These results are in accord with previous studies on the homologous protein, calbindin D_{9k}, showing the effect on stability of repulsive interactions between negative charges (*57*). Since the degree of stabilization is not quantified in the present case, the energy levels of the apo states of E104Q and E140Q are chosen at arbitrary values lower than for apo wt-TR_2C (Figure 6).

E104Q and E140Q bind Ca^{2+} essentially sequentially which enables us to gain information about the intermediate $(Ca^{2+})_1$ states (Table 1). In addition to the very weakened Ca^{2+} binding in the mutated loop, the Ca^{2+} affinity for the first ion also is decreased for both mutants compared to wt-TR_2C. As stated above, the macroscopic binding constants are assumed to be equal to the site-specific microscopic binding constants, i.e. $K_1 = k_{IV} = 5.3 \pm 0.2$ and $K_2 = k_{III,IV} = 2.94 \pm 0.06$ for E104Q and $K_1 = k_{III} = 4.5 \pm 0.3$ and $K_2 = k_{IV,III} = 3.15 \pm 0.10$ for E140Q (*28*). Using these relations, a comparison of the Ca^{2+} affinities reveals that loop IV binds Ca^{2+} relatively stronger, i.e. $k_{IV} > k_{III}$ and $k_{IV,III} > k_{III,IV}$. This finding is consistent with the charge characteristics of the binding loops—loop IV has a net charge of -5 and four charged Ca^{2+} ligands while loop III only has a net charge of -2 and three charged Ca^{2+} ligands. Thus, it appears that loop IV is likely to bind preferentially the first Ca^{2+} in the C-terminal domain of wild-type CaM.

Several observations concerning the loop regions in the mutants may as well be applicable for the wild-type protein, e.g. the structural rearrangements of the empty binding loops of the $(Ca^{2+})_1$ states of E104Q and E140Q. Substantial chemical shifts changes toward the values for $(Ca^{2+})_2$ wt-TR_2C are observed for residues in the first half of the empty loops, i.e. D93−G98 in $(Ca^{2+})_1$ E104Q and D129−G134 in $(Ca^{2+})_1$ E140Q (Figure 4A). Preformation of the empty loop toward a conformation similar to that when Ca^{2+} is bound is hence indicated, which may contribute to the positive cooperativity in Ca^{2+} binding. Since such loop displacement also is seen for the seemingly closed $(Ca^{2+})_1$ state of E140Q, interactions between the binding loops, most likely transmitted via the β-sheet, seem to be of importance. The Ca^{2+}-induced conformational change in the loop in regulatory EF-hand proteins involves a flexible motion pivoting on the middle residue in the β-strand, decreasing the length of the β-sheet and serving to bring the ends of the loop together to coordinate the Ca^{2+} (*17*).

The present results provide some important clues to the molecular events behind the strong cooperative Ca^{2+} binding and Ca^{2+}-induced structural changes in CaM. A plausible mechanism in wt-TR_2C would be that already when Ca^{2+} binds first to loop IV, most of the structural and dynamical changes characterizing the $(Ca^{2+})_2$ state take place, e.g. the exposure of the hydrophobic patch and preformation of loop III. This mechanism was observed in NMR studies of calbindin D_{9k} where the intermediate state was studied using Cd^{2+} (*58*). The size of Ca^{2+}-induced structural changes in calbindin D_{9k} are small compared to CaM, but both the 3D structure (*59*) and the dynamics (*60*) of the $(Cd^{2+})_1$ state are significantly more similar to the $(Ca^{2+})_2$ state (*61*) than to the apo state (*62*). The binding of the second Ca^{2+} to wt-TR_2C is thus facilitated and stabilizes the open conformation by counterbalancing the repulsive interactions between the negatively charged side-chains in loop III. These studies support such a model, since large global rearrangements seem to occur when Ca^{2+} binds to loop IV and this loop also seems to be the stronger binding site. The minor structural changes in $(Ca^{2+})_1$ E140Q, with Ca^{2+} bound to loop III, either mimic the situation in wt-TR_2C or reveal a critical role for E140 when Ca^{2+} binds to loop III. In calbindin D_{9k}, major structural changes seem to occur upon binding of the first ion, independent of which loop it binds to (*63*).

Schematically, helices E and H alter their interaction mainly by rotations about the helical axis while helices F and G swing out from helices E and H to yield the open conformation when Ca^{2+} binds to wt-TR_2C. When the side-chain of E140 coordinates the Ca^{2+}, helix H is forced to rotate and thereby its interaction with helix E changes. The aromatic side-chain of F141, interacting with side-chains from helices F and G in the apo state, is pulled into the interface between helices E and H (Figure 7). Rotation of helix E is achieved by changing the C-terminus from a 3_{10}- to an α-helix. Such a conformation may perhaps contribute to the apparent preformation of loop III. The concomitant displacement of F92 completes formation of the stabilizing aromatic cluster between helices E and H. If the same changes occur when the first Ca^{2+} binds to loop IV in E104Q, it would explain why helix E displays large chemical shift changes (Figure 3A). When the second Ca^{2+} binds to loop III, extra structural changes occur, primarily in the N-terminal EF-hand (Figures 3B and 4). Helix G seems affected mainly by Ca^{2+} binding to loop IV.

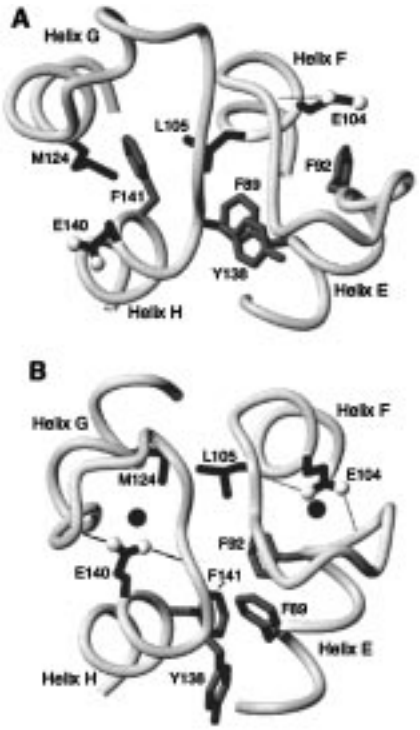

FIGURE 7: Panels A and B show the central part of the 3D structures of the apo state (*13*) and $(Ca^{2+})_2$ state (*10*) of the C-terminal domain of CaM. The positions of some important side-chains in the two states are indicated in more detail. Hydrogen bonds formed from the side-chains of E104 and E140 are shown as dashed lines.

Conformational Exchange, and the Bidentate Ca^{2+} Ligand. The studies of E104Q and E140Q show that mutation of the glutamic acid in the 12th position of either of the two binding loops has large effects on the structures of the Ca^{2+}-loaded states and the Ca^{2+} affinities. As stated above, NOE data indicate that $(Ca^{2+})_2$ E140Q as well as the $(Ca^{2+})_1$ and $(Ca^{2+})_2$ states of E104Q experience exchange between conformations, similar to the closed and open states of wt-TR_2C. Such an exchange would explain why the majority of the observed chemical shifts for these states lie between the apo and $(Ca^{2+})_2$ chemical shifts of wt-TR_2C, as well as the occurrence of broadened resonances. The results may shed light on an earlier NMR study of an equivalent mutant of calbindin D_{9k} where the $(Ca^{2+})_2$ state was reported to be different from the wild-type protein as indicated by large chemical shift deviations (*23*). Perhaps this mutant also undergoes conformational exchange but, due to the relatively subtle Ca^{2+}-induced structural rearrangements in calbindin D_{9k}, such an exchange will be hard to reveal from NOE data.

Chemical shift data and NOE data both indicate that the mutation increases the free energy of the open $(Ca^{2+})_2$ state to a level approximately identical to the free energy of a closed $(Ca^{2+})_2$ state so that both substates become significantly populated. An explanation for the destabilization of the open conformation may be the inability of the mutated side-chain to form all of the hydrogen bonds observed in $(Ca^{2+})_2$ wt-TR_2C (*64*) (Figure 7). For E140Q, we discussed the possibility of alternating hydrogen bonding, with a hydrogen bond between Q140 and N137 in the closed conformation (*28*), consistent with the 3D structure of apo CaM (*13*). In the open conformation, the side-chain of Q140 could reorient to form a hydrogen bond to I130, associated with the altered orientation of the ring of F141 and the formation of the aromatic cluster. How the Ca^{2+} coordination is achieved in the two different conformations is still not elucidated, but the chemical shifts indicate that Ca^{2+} ligands are provided from the side-chains of residues in loop positions 1, 3, and 5. Furthermore, the ^{15}N chemical shift of V136 (124.2 ppm) indicates that the backbone oxygen of Q135 in position 7 of loop IV coordinates Ca^{2+} (*65*), and the corresponding Ca^{2+} ligation in loop III by Y99 appears to be present at least part of the time (the ^{15}N chemical shift of I100 is 121.2 ppm). The glutamine in the twelfth position may either coordinate via the side-chain oxygen or via a water molecule—perhaps differently in the closed and open state. The new results for E104Q strongly indicate that bidentate Ca^{2+} coordination of both glutamic acid residues and all their hydrogen bonds is required to stabilize the protein in the open conformation. The importance of the bidentate Ca^{2+} ligands is also emphasized in studies of a mutated N-terminal fragment of smooth muscle TnC, where the bidentate glutamic acid in loop I was changed to an alanine (*66*, *67*). No hydrogen bonding or Ca^{2+} coordination can be performed by the alanine side-chain, and the Ca^{2+}-saturated state of the domain was found to be closed. Together these results highlight the delicate balance between Ca^{2+} coordination and hydrogen bonds within the loops and their importance to maintaining the open conformation.

Although the NOEs are indicative of exchange between a closed and an open conformation, we cannot exclude the presence of significantly populated states with intermediate conformations. It is interesting to note that certain nuclei in the β-sheet and helices F and G experience chemical shift changes in the opposite direction as compared to wt-TR_2C, suggesting new local chemical environments for these nuclei due to the bound Ca^{2+} in the closed conformation and/or the presence of some other significantly populated states. A simple model, which may fit the experimental results but would be hard to prove, is that each EF-hand changes individually between a closed and open conformation. Although the two EF-hands most likely couple, so that open−open or closed−closed conformations are preferred, open−closed and closed−open conformations may also be populated. Compared to helices E and H, helices F and G change their relative orientation significantly more upon Ca^{2+} binding. If only one of the two EF-hands is open, the resulting interaction between helices F and G would perhaps contribute in a nonwild-type-like way to the observed chemical shifts. On the other hand, complex reactions, e.g. global conformational exchange in a protein, are likely to occur in a rugged energy landscape with a number of local minima (*68*−*70*). In our case, the closed and open substates would be represented by two energy minima, but also other conformational substates could be significantly populated.

The structure calculations of $(Ca^{2+})_2$ E104Q resulted in an essentially closed conformation for the ensemble of 50 determined 3D structures. Without any knowledge about the wild-type structures one might be led to conclude that $(Ca^{2+})_2$ E104Q experiences large scale motions around a single conformation that would be represented by the calculated structures. It is expected, however, that structures will be well-defined due to pinning when counteracting sets of distance restraints have to be fulfilled and no provision for exchange is included. The bent helix F and the poor quality of helix G and the β-sheet also indicate that the

structures are unrealistic. With the large number of violations and strong evidence of chemical exchange in mind, we believe that the calculated ensemble represents an artificial average structure rather than the real structures of $(Ca^{2+})_2$ E104Q. The use of ensemble- or time-averaged treatment of the NOEs in the structure calculations would be the natural next step to obtain more physically relevant structures of the open and closed conformations.

CONCLUSIONS

The present results provide a good illustration of the different roles played by the N-terminal and C-terminal EF-hands in an EF-hand pair domain. In E104Q, binding of the first Ca^{2+} to the C-terminal EF-hand results in substantial structural changes. It must be emphasized, however, that even if both the $(Ca^{2+})_1$ and $(Ca^{2+})_2$ states of E104Q seem to experience conformational exchange, significant chemical shift changes occur upon binding of the second Ca^{2+}. In contrast, the binding of the first Ca^{2+} to the N-terminal EF-hand in E140Q gives rise to small effects while the second C-terminal Ca^{2+} binding causes large structural rearrangements. The final $(Ca^{2+})_2$ states of both mutants are similar with respect to the chemical shifts and the global conformational interchange at a 10−100 μs time scale. This shows that even if the two EF-hands play different roles for the structural rearrangements of the protein, both E104 and E140 are important for the stabilization of the Ca^{2+}-activated open structure of CaM.

ACKNOWLEDGMENT

We thank Drs. Mikael Akke, Torbjörn Drakenberg, and Peter Sellers for valuable comments and stimulating discussions. Dr. Garry Gippert is gratefully acknowledged for helpful assistance using GENXPK and POSER.

SUPPORTING INFORMATION AVAILABLE

A table of the backbone ^1H and ^{15}N amide assignments of the apo, $(Ca^{2+})_1$, and $(Ca^{2+})_2$ states of E104Q (2 pages). Ordering information is given on any current masthead page.

REFERENCES

1. Evenäs, J., Malmendal, A., and Forsén, S. (1998) *Curr. Opin. Chem. Biol. 2*, 293−302.
2. Berridge, M. J. (1997) *J. Physiol. (London) 499*, 290−306.
3. Kretsinger, R. H., and Nockolds, C. E. (1973) *J. Biol. Chem. 248*, 3313−3326.
4. Henikoff, S., Greene, E. A., Pletrokovski, S., Bork, S., and Attwood, T. K. (1997) *Science 278*, 609−614.
5. Klee, C. B. (1988) in *Molecular Aspects of Cellular Regulation* (Cohen, P., and Klee, C. B., Eds.) pp 35−56, Elsevier, New York.
6. Crivici, A., and Ikura, M. (1995) *Annu. Rev. Biophys. Biomol. Struct. 24*, 85−116.
7. Finn, B. E., and Forsén, S. (1995) *Structure 3*, 7−11.
8. Celio, M. R., Pauls, T., and Schwaller, B. (1996) *Guidebook to the calcium-binding proteins*, 1st ed., Oxford University Press, Oxford, U.K.
9. Barbato, G., Ikura, M., Kay, L. E., Pastor, R. W., and Bax, A. (1992) *Biochemistry 31*, 5269−78.
10. Babu, Y. S., Bugg, C. E., and Cook, W. J. (1988) *J. Mol. Biol. 204*, 191−204.
11. Chattopadhyaya, R., Meador, W. E., Means, A. R., and Quiocho, F. A. (1992) *J. Mol. Biol. 228*, 1177−92.
12. Ikura, M., Clore, G. M., Gronenborn, A. M., Zhu, G., Klee, C. B., and Bax, A. (1992) *Science 256*, 632−8.
13. Kuboniwa, H., Tjandra, N., Grzesiek, S., Ren, H., Klee, C. B., and Bax, A. (1995) *Nature Struct. Biol. 2*, 768−776.
14. Zhang, M., Tanaka, T., and Ikura, M. (1995) *Nature Struct. Biol. 2*, 758−767.
15. Herzberg, O., and James, M. N. G. (1988) *J. Mol. Biol. 203*, 761−779.
16. Gagné, S. M., Tsuda, S., Li, M. X., Smillie, L. B., and Sykes, B. D. (1995) *Nature Struct. Biol. 2*, 784−789.
17. Strynadka, N. C. J., Cherney, M., Sielicki, A. R., Li, M. X., Smillie, L. B., and James, M. N. G. (1997) *J. Mol. Biol. 273*, 238−255.
18. Walsh, M., Stevens, F. C., Kuznicki, J., and Drabikowski, W. (1977) *J. Biol. Chem. 252*, 7440−7443.
19. Drabikowski, W., Kuznicki, J., and Grabarek, Z. (1977) *Biochim. Biophys. Acta 485*, 124−133.
20. Finn, B. E., Evenäs, J., Drakenberg, T., Waltho, J. P., Thulin, E., and Forsén, S. (1995) *Nature Struct. Biol. 2*, 777−783.
21. Linse, S., Helmersson, A., and Forsén, S. (1991) *J. Biol. Chem. 266*, 8050−4.
22. Beckingham, K. (1991) *J. Biol. Chem. 266*, 6027−30.
23. Carlström, G., and Chazin, W. J. (1993) *J. Mol. Biol. 231*, 415−30.
24. Maune, J. F., Beckingham, K., Martin, S. R., and Bayley, P. M. (1992) *Biochemistry 31*, 7779−86.
25. Maune, J. F., Klee, C. B., and Beckingham, K. (1992) *J. Biol. Chem. 267*, 5286−95.
26. Shea, M. A., Verhoeven, A. S., and Pedigo, S. (1996) *Biochemistry 35*, 2943−2957.
27. Martin, S. R., Maune, J. F., Beckingham, K., and Bayley, P. M. (1992) *Eur. J. Biochem. 205*, 1107−1114.
28. Evenäs, J., Thulin, E., Malmendal, A., Forsén, S., and Carlström, G. (1997) *Biochemistry 36*, 3448−3457.
29. Brodin, P., Grundström, T., Hofmann, T., Drakenberg, T., Thulin, E., and Forsén, S. (1986) *Biochemistry 25*, 5371−5377.
30. Aue, W. P., Batholdi, E., and Ernst, R. R. (1976) *J. Chem. Phys. 64*, 2229−2246.
31. Macura, S., and Ernst, R. R. (1980) *Mol. Phys. 41*, 95−117.
32. Bax, A. (1985) *J. Magn. Reson. 65*, 142−145.
33. Braunschweiler, L., Bodenhausen, G., and Ernst, R. R. (1983) *Mol. Phys. 48*, 535−560.
34. Braunschweiler, L., and Ernst, R. R. (1983) *J. Magn. Reson. 53*, 521−528.
35. Shaka, A. J., Lee, C. J., and Pines, A. (1988) *J. Magn. Reson. 77*, 274−293.
36. Cavanagh, J., and Rance, M. (1992) *J. Magn. Reson. 96*, 670−678.
37. Zhang, O., Kay, L. E., Olivier, J. P., and Forman-Kay, J. D. (1994) *J. Biomol. NMR 4*, 845−858.
38. Shaka, A. J., Keeler, J., Frenkiel, T., and Freeman, R. (1983) *J. Magn. Reson. 52*, 335−338.
39. Hartel, A. J., Lankhorst, P. P., and Altona, C. (1982) *Eur. J. Biochem. 129*, 343−357.
40. Orbons, L. P. M., van der Marel, G. A., van Boom, J. H., and Altona, C. (1987) *Eur. J. Biochem. 170*, 225−239.
41. Wishart, D. S., Bigam, C. G., Yao, J., Abildgaard, F., Dyson, H. J., Oldfield, E., Markley, J. L., and Sykes, B. D. (1995) *J. Biomol. NMR 6*, 135−140.
42. Gippert, G. P. (1995) Ph.D. Thesis, The Scripps Research Institute, San Diego. Source code for GENXPK available at http://www.fkem2.lth.se/∼garry/programs.html.
43. Finn, B. E., Drakenberg, T., and Forsén, S. (1993) *FEBS Lett. 336*, 368−374.
44. Chazin, W. J., and Wright, P. E. (1987) *Biopolymers 26*, 973−977.
45. Sandström, J. (1982) *Dynamic NMR Spectroscopy*, 1 ed., Academic Press Inc., London.
46. Brünger, A. T. (1992) *X-PLOR, Version 3.1. A System for X-ray Crystallography and NMR*, Yale University Press, New Haven, CT.
47. Nilges, M., Clore, G. M., and Gronenborn, A. M. (1988) *FEBS Lett. 229*, 317−324.

48. Nilges, M. A. (1993) *Proteins Struct. Funct. Genet. 17*, 295−309.
49. Tropp, J. (1980) *J. Chem. Phys. 72*, 6035−6043.
50. Koning, T. M. G., Boelens, R., and Kaptein, R. (1990) *J. Magn. Res. 90*, 111−123.
51. Linse, S., Thulin, E., and Sellers, P. (1993) *Protein Sci. 2*, 985−1000.
52. Seamon, K. B. (1980) *Biochemistry 19*, 207−215.
53. Laskowski, R. A., MacArthur, M. W., Moss, D. S., and Thornton, J. M. (1993) *J. Appl. Crystallogr. 26*, 283−291.
54. Kessler, H., Griesinger, C., Lautz, J., Müller, A., van Gunsteren, W. F., and Berendsen, H. J. C. (1988) *J. Am. Chem. Soc. 110*, 3393−3396.
55. Torda, A. E., Scheek, R. M., and van Gunsteren, W. F. (1990) *J. Mol. Biol. 214*, 223−235.
56. Bonvin, A. M. J. J., Boelens, R., and Kaptein, R. (1994) *J. Biomol. NMR 4*, 143−149.
57. Akke, M., and Forsén, S. (1990) *Proteins: Struct., Funct., Genet. 8*, 23−29.
58. Akke, M., Forsén, S., and Chazin, W. J. (1991) *J. Mol. Biol. 220*, 173−89.
59. Akke, M., Forsén, S., and Chazin, W. J. (1995) *J. Mol. Biol. 252*, 102−121.
60. Akke, M., Skelton, N. J., Kördel, J., Palmer, A. G., and Chazin, W. J. (1993) *Biochemistry 32*, 9832−44.
61. Kördel, J., Skelton, N. J., Akke, M., and Chazin, W. J. (1993) *J. Mol. Biol. 231*, 711−34.
62. Skelton, N. J., Kördel, J., and Chazin, W. J. (1995) *J. Mol. Biol. 249*, 441−462.
63. Wimberly, B., Thulin, E., and Chazin, W. J. (1995) *Protein Sci. 4*, 1045−1055.
64. Strynadka, N. C. J., and James, M. N. G. (1989) *Annu. Rev. Biochem. 58*, 951−998.
65. Biekofsky, R. B., Martin, S. R., Browne, J. P., Bayley, P. M., and Feeney, J. (1998) *Biochemistry 37*, 7617−7629.
66. Gagné, S. M., Li, M. X., and Sykes, B. D. (1997) *Biochemistry 36*, 4386−4392.
67. Li, M. X., Gagné, S. M., Spyracopoulos, L., Kloks, C. P. A. M., Audette, G., Chandra, M., Solaro, R. J., Smillie, L. B., and Sykes, B. D. (1997) *Biochemistry 36*, 12519−12525.
68. Zwanzig, R. (1988) *Proc. Natl. Acad. Sci. U.S.A. 85*, 2029−2030.
69. Frauenfelder, H., Sligar, S. G., and Wolynes, P. G. (1991) *Science 254*, 1598−1603.
70. Denisov, V. P., Peters, J., Hörlein, H. D., and Halle, B. (1996) *Nature Struct. Biol. 3*, 505−509.

BI9806448